Inorg. Chem. **2006**, *45*, 5529–5537

Directed Synthesis of Noncentrosymmetric Molybdates Using Composition Space Analysis

Thomas R. Veltman,[†] Adam K. Stover,[†] Amy Narducci Sarjeant,[‡] Kang Min Ok,[§] P. Shiv Halasyamani,[§] and Alexander J. Norquist*,[†]

Department of Chemistry, Haverford College, Haverford, Pennsylvania 19041, Department of Chemistry, University of Houston, Houston, Texas 77204-5003, and Department of Chemistry, Johns Hopkins University, Baltimore, Maryland 21218

Received April 3, 2006

A systematic investigation of the factors governing the reaction product composition, hydrogen bonding, and symmetry was conducted in the MoO_3/3-aminoquinuclidine/H_2O system. Composition space analysis was performed through 36 individual reactions under mild hydrothermal conditions using racemic 3-aminoquinuclidine. Single crystals of three new compounds, $[C_7H_{16}N_2][Mo_3O_{10}]\cdot H_2O$, $[C_7H_{16}N_2]_2[Mo_8O_{26}]\cdot H_2O$, and $[C_7H_{16}N_2]_2[Mo_8O_{26}]\cdot 4H_2O$, were grown. The relative phase stabilities for these products are dependent upon the reactant mole fractions in the initial reaction gel. This phase stability information was used to direct the synthesis of two new noncentrosymmetric compounds, using either (*S*)–(–)-3-aminoquinuclidine dihydrochloride or (*R*)-(+)-3-aminoquinuclidine dihydrochloride. $[(R)\text{-}C_7H_{16}N_2]_2[Mo_8O_{26}]$ and $[(S)\text{-}C_7H_{16}N_2]_2[Mo_8O_{26}]$ both crystallize in the noncentrosymmetric space group $P2_1$ (No. 4), which has the polar crystal class 2 (C_2). The second-harmonic generation activities were measured on sieved powders. The structure-directing properties of the molybdate components in each compound were determined using bond valence sums. The structures of all five compounds were determined using single-crystal X-ray diffraction.

Introduction

Conducting reactions under hydrothermal conditions is a well-established method for the preparation of inorganic structures templated by organic cations.[1−9] Despite the vast amount of effort expended upon such studies, true control over the product composition and structure often remains elusive.

Composition space analysis[10−13] is known to be a viable technique for the elucidation of the factors governing the reaction product composition. Composition space analysis involves the introduction of subtle variations in the reactant concentrations over a series of analogous experiments. All other reaction variables, such as temperature and reaction time, are held constant, enabling direct observation of the effects that result from these composition differences. Bond valence sums[14] can be used to educe the structure-directing properties of inorganic architectures, through quantification of the relative nucleophilicities of each potential hydrogen-bond acceptor. The ubiquitous hydrogen-bonding networks in such compounds are largely dependent upon the structure-directing properties of the anions. Product symmetry is of special interest to researchers owing to several symmetry-dependent[15] physical properties:[16] enantiomorphism, optical activity (circular dichroism), piezoelectricity, pyroelectricity,

* To whom correspondence should be addressed. E-mail: anorquis@haverford.edu.
[†] Haverford College.
[‡] Johns Hopkins University.
[§] University of Houston.

(1) Cheetham, A. K.; Férey, G.; Loiseau, T. *Angew. Chem., Int. Ed.* **1999**, *38*, 3268.
(2) Fernandez, S. J.; Mesa, L.; Pizarro, J. L.; Lezama, L.; Arriortura, M. I.; Rojo, T. *Chem. Mater.* **2002**, *14*, 2300.
(3) Walker, S. M.; Halasyamani, P. S.; O'Hare, D. *J. Am. Chem. Soc.* **1999**, *121*, 7415.
(4) Reisner, B. A.; Tripathi, A.; Parise, J. B. *J. Mater. Chem.* **2001**, *11*, 887.
(5) Bu, X.; Feng, P.; Gier, T. E.; Zhao, D.; Stucky, G. D. *J. Am. Chem. Soc.* **1998**, *120*, 13389.
(6) Ekambarem, S.; Sevov, S. *Inorg. Chem.* **2000**, *39*, 2405.
(7) Vaidhyanathan, R.; Natarajan, S.; Rao, C. N. R. *Inorg. Chem.* **2002**, *17*, 4496.
(8) Choudhury, A.; Kumar, U.; Rao, C. N. R. *Angew. Chem., Int. Ed.* **2002**, *41*, 158.
(9) Harrison, W. T. A.; Phillips, M. L. F.; Stanchfield, J.; Nenoff, T. M. *Angew. Chem., Int. Ed.* **2000**, *39*, 3808.
(10) Halasyamani, P. S.; Willis, M. J.; Stern, C. L.; Lundquist, P. M.; Wong, G. K.; Poeppelmeier, K. R. *Inorg. Chem.* **1996**, *35*, 1367.
(11) Harrison, W. T. A.; Dussack, L. L.; Jacobson, A. J. *J. Solid State Chem.* **1996**, *125*, 234.
(12) Norquist, A. J.; Heier, K. R.; Stern, C. L.; Poeppelmeier, K. R. *Inorg. Chem.* **1998**, *37*, 6495.
(13) Doran, M. B.; Norquist, A. J.; O'Hare, D. *Inorg. Chem.* **2003**, *42*, 6989.
(14) Brown, I. D.; Altermatt, D. *Acta Crystallogr., Sect. B* **1985**, *41*, 244.
(15) Chen, C.; Liu, G. *Annu. Rev. Mater. Sci.* **1986**, *16*, 203.
(16) Halasyamani, P. S.; Poeppelmeier, K. R. *Chem. Mater.* **1998**, *10*, 2753.

10.1021/ic060558t CCC: $33.50
Published on Web 06/10/2006

Table 1. Crystallographic Data for Compounds **1**−**5**

compd	$[C_7H_{16}N_2][Mo_3O_{10}]\cdot H_2O$ (**1**)	$[C_7H_{16}N_2]_2[Mo_8O_{26}]\cdot H_2O$ (**2**)	$[C_7H_{16}N_2]_2[Mo_8O_{26}]\cdot 4H_2O$ (**3**)	$[(R)\text{-}C_7H_{16}N_2]_2[Mo_8O_{26}]$ (**4**)	$[(S)\text{-}C_7H_{16}N_2]_2[Mo_8O_{26}]$ (**5**)
formula	$C_7H_{16}Mo_3N_2O_{11}$	$C_{14}H_{34}Mo_8N_4O_{27}$	$C_{14}H_{40}Mo_8N_4O_{30}$	$C_{14}H_{32}Mo_8N_4O_{26}$	$C_{14}H_{32}Mo_8N_4O_{26}$
fw	591.90	1457.95	1512.00	1439.94	1439.94
space group	$P2_1/m$ (No. 10)	$Pbcn$ (No. 60)	$P2_1/n$ (No. 14)	$P2_1$ (No. 4)	$P2_1$ (No. 4)
a/Å	8.890(2)	12.7611(8)	7.9547(3)	7.2672(3)	7.2685(3)
b/Å	7.6605(8)	16.2554(12)	11.0404(5)	11.6360(5)	11.6423(5)
c/Å	10.6695(13)	15.6322(11)	20.6373(7)	19.6965(8)	19.6887(9)
β/deg	103.541(15)	90	94.684(3)	99.852(4)	99.948(4)
V/Å^3	706.4(2)	3242.7(4)	1806.38(12)	1641.00(12)	1641.05(13)
Z	2	4	2	2	2
ρ_{calcd}/g cm^{-3}	2.782	2.986	2.780	2.914	2.914
λ/Å	0.71073	0.71073	0.71073	0.71073	0.71073
T/K	110(2)	110(2)	110(2)	110(2)	110(2)
μ/mm^{-1}	2.683	3.101	2.794	3.060	3.060
total reflns	5412	54098	32095	26377	25828
independent reflns	1913	4896	7288	8344	8087
obsd reflns	1296 [$I > 3\sigma$]	3153 [$I > 3\sigma$]	5181 [$I > 3\sigma$]	6144 [$I > 3\sigma$]	5977 [$I > 3\sigma$]
param	148	243	254	471	471
Flack param				−0.07(4)	−0.08(5)
R1[a]	0.0326	0.0210	0.0208	0.0211	0.0225
wR2[b]	0.0743	0.0426	0.0440	0.0382	0.0438

[a] $R1 = \sum||F_o| - |F_c||/\sum|F_o|$. [b] $wR2 = [\sum w(F_o^2 - F_c^2)^2/[\sum w(F_o^2)^2]^{1/2}$.

and second-order nonlinear-optical activity [second-harmonic generation (SHG)]. Several strategies[17−20] are currently employed to direct noncentrosymmetry in new crystalline compounds, including the use of chiral organic amines.[21,22]

A systematic investigation of the MoO_3/3-aminoquinuclidine/H_2O system was conducted to probe the factors dictating product composition, the structure-directing properties of the inorganic component (and related hydrogen-bonding networks), and the product symmetry. The synthesis, structure, and characterization of five novel organically templated molybdates, two of which are noncentrosymmetric, are reported.

Experimental Section

Materials. MoO_3 (99.5%, Aldrich), H_2SO_4 (98%, Aldrich), 3-aminoquinuclidine dihydrochloride (aqn; 98%, Aldrich), (*S*)-(−)-3-aminoquinuclidine dihydrochloride (*S*-aqn; 98%, Aldrich), and (*R*)-(+)-3-aminoquinuclidine dihydrochloride (*R*-aqn; 98%, Aldrich) were used as received. Deionized water was used in these syntheses.

Synthesis. All reactions were conducted in 23-mL poly(fluoroethylenepropylene)-lined pressure vessels. Reactions were heated to 180 °C over 30 min and allowed to soak for 24 h. The reactions were then cooled to room temperature at a rate of 6 °C h^{-1}. Autoclaves were opened in air, and products were recovered through filtration. Reaction yields ranged between 30 and 60%, based upon molybdenum. No additional reaction products other than those described below, crystalline or amorphous, were observed.

$[C_7H_{16}N_2][Mo_3O_{10}]\cdot H_2O$ (**1**) was synthesized through the reaction of 0.1415 g (9.83×10^{-4} mol) of MoO_3, 0.8138 g (4.092×10^{-3} mol) of aqn, 0.1993 g (2.034×10^{-3} mol) of H_2SO_4, and 1.9998 g (1.111×10^{-1} mol) of deionized water. Colorless needles were recovered. Elem microanal. Obsd for **1** (calcd): C, 14.39 (14.19); H, 2.66 (2.70); N, 4.79 (4.73). IR data (cm^{-1}): ν(N−H) 3113, 1589, ν(C−H) 1466, ν(M═O) 921.

$[C_7H_{16}N_2]_2[Mo_8O_{26}]\cdot H_2O$ (**2**) was synthesized through the reaction of 0.5868 g (4.077×10^{-3} mol) of MoO_3, 0.2164 g (1.088×10^{-3} mol) of aqn, 0.2164 g (2.208×10^{-3} mol) of H_2SO_4, and 1.0015 g (5.5564×10^{-2} mol) of deionized water. Colorless blocks were recovered. Elem microanal. Obsd for **2** (calcd): C, 11.81 (11.52); H, 2.16 (2.33); N, 3.91 (3.84). IR data (cm^{-1}): ν(N−H) 3136, 1621, ν(C−H) 1491, ν(M═O) 967.

$[C_7H_{16}N_2]_2[Mo_8O_{26}]\cdot 4H_2O$ (**3**) was synthesized through the reaction of 0.4603 g (3.198×10^{-3} mol) of MoO_3, 0.4041 g (2.032×10^{-3} mol) of aqn, 0.2099 g (2.142×10^{-3} mol) of H_2SO_4, and 1.0358 g (5.754×10^{-2} mol) of deionized water. Light-green blocks were recovered. Elem microanal. Obsd for **3** (calcd): C, 11.14 (11.11); H, 2.48 (2.64); N, 3.71 (3.70). IR data (cm^{-1}): ν(N−H) 3105, 1618, ν(C−H) 1473, ν(M═O) 957.

$[(R)\text{-}C_7H_{16}N_2]_2[Mo_8O_{26}]$ (**4**) was synthesized through the reaction of 0.3897 g (2.70×10^{-3} mol) of MoO_3, 0.03520 g (1.77×10^{-3} mol) of *R*-aqn, 0.1428 g (1.457×10^{-3} mol) of H_2SO_4, and 1.0107 g (5.615×10^{-2} mol) of deionized water. Colorless blocks were recovered. Elem microanal. Obsd for **4** (calcd): C, 11.66 (11.66); H, 2.10 (2.22); N, 3.92 (3.88). IR data (cm^{-1}): ν(N−H) 3120, 1607, ν(C−H) 1487, ν(M═O) 975.

$[(S)\text{-}C_7H_{16}N_2]_2[Mo_8O_{26}]$ (**5**) was synthesized through the reaction of 0.4102 g (2.85×10^{-3} mol) of MoO_3, 0.2411 g (1.212×10^{-3} mol) of *S*-aqn, 0.1603 g (1.636×10^{-3} mol) of H_2SO_4, and 1.0050 g (5.583×10^{-2} mol) of deionized water. Colorless blocks were recovered. Elem microanal. Obsd for **5** (calcd): C, 11.63 (11.66); H, 2.14 (2.22); N, 3.91 (3.88). IR data (cm^{-1}): ν(N−H) 3121, 1607, ν(C−H) 1460, ν(M═O) 972.

Powder X-ray diffraction patterns of each bulk sample match the pattern generated from the respective single-crystal X-ray structure data.

Single-Crystal X-ray Diffraction. Data were collected using an Oxford Diffraction Xcalibur3 CCD diffractometer with Enhance Mo Kα radiation (λ = 0.710 73 Å). A single crystal was mounted on a glass fiber using *N*-paratone oil and cooled in situ to 110(2) K for data collection. Frames were collected, indexed, and processed and the files scaled using *CrysAlis RED*.[23] The heavy-atom positions were determined using SIR92.[24] All other non-hydrogen sites were located from Fourier difference maps. All non-hydrogen sites were refined using anisotropic thermal parameters using full-matrix least-squares procedures on F_o^2 with $I > 3\sigma(I)$. Hydrogen atoms were placed in geometrically idealized positions. All calculations were performed using Crystals.[25] Relevant crystallographic data are listed in Table 1.

(17) Halasyamani, P. S. *Chem. Mater.* **2004**, *16*, 3586.
(18) Kwon, Y. U.; Lee, K. S.; Kim, Y. H. *Inorg. Chem.* **1996**, *35*, 1161.

Powder X-ray Diffraction. Powder diffraction patterns were recorded on a GBC-Difftech MMA powder diffractometer. Samples were mounted on aluminum plates. Calculated powder patterns were generated from single-crystal data using *ATOMS*, version 6.0.[26]

Infrared Spectroscopy. Infrared measurements were obtained using a Perkin-Elmer Fourier transform infrared Spectrum 1000 spectrophotometer. Samples were diluted with spectroscopic-grade KBr and pressed into a pellet. A scan was run over the range of 400−4000 cm^{-1}.

Nonlinear-Optical Measurements. Powder SHG measurements were conducted using a modified Kurtz-NLO system, with a 1064-nm light source.[27,28] Polycrystalline **4** and **5** were ground and sieved into distinct particle size ranges: <20, 20−45, 45−63, 63−75, 75−90, and 90−120 μm. Crystalline α quartz was ground and sieved into identical particle size ranges in order to compare the SHG properties of **4** and **5** with known materials. All powders were placed in separate capillary tubes; no index-matching fluid was used in any experiment. The SHG, i.e., 532-nm light, was collected in reflection and detected using a photomultiplier tube. A 532-nm narrow-band-pass interference filter was attached to the tube in order to only detect the SHG light.

Results

The inorganic components present in compounds **1**−**5** vary in dimensionality and connectivity. Certain structural features are, however, retained. Each second-order Jahn−Teller active molybdenum(VI) is six-coordinate, in a distorted octahedral geometry. Mo−$O_{terminal}$ bonds are generally shorter than Mo−$O_{bridging}$ bonds; the observed ranges are 1.687(4)−1.737(6) and 1.746(4)−2.460(2) Å, respectively. A much wider spread in Mo−$O_{bridging}$ bonds is observed because the bridging oxides can be shared by two, three, four, or five neighboring molybdenum centers.

1. Two distinct molybdenum environments are present in this compound. The MoO_6 coordination octahedra containing Mo1 share common edges with four adjacent MoO_6 octahedra, all of which contain Mo2 (see Figure 1). In contrast, the MoO_6 coordination octahedra that contain Mo2 share two common edges with adjacent Mo1 octahedra and a single edge with a Mo2-containing MoO_6 octahedron, resulting in the formation of extended chains that exhibit the formula $[Mo_3O_{10}]_n^{2n-}$. This chain connectivity has been previously reported.[29−31] These chains are aligned in the [0 1 0] direction, while successive chains lie next to one another in the *ab* plane. A single disordered $[aqnH_2]^{2+}$ cation is present in the asymmetric unit, which is comprised of both a [*R*-$aqnH_2]^{2+}$ and a [*S*-$aqnH_2]^{2+}$ cation. The disorder mechanism is shown in Figure 2.

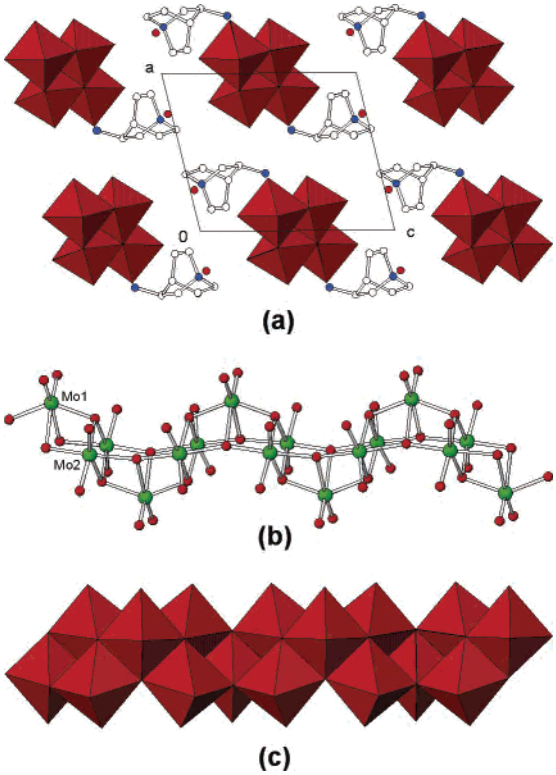

Figure 1. (a) Three-dimensional packing of **1**. Red octahedra represent MoO_6, while white, blue, and red circles represent carbon, nitrogen, and oxygen atoms, respectively. The unit cell is shown. Ball-and-stick (b) and polyhedral (c) representation of the $[Mo_3O_{10}]_n^{2n-}$ chains in **1**.

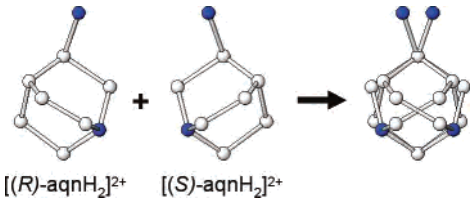

Figure 2. Disorder mechanism present in the [*R*-$aqnH_2]^{2+}$ and [*S*-$aqnH_2]^{2+}$ cations in **1**.

2. The β-octamolybdate anions, $[Mo_8O_{26}]^{4-}$, observed in **2** are well-known.[32−34] Four unique molybdenum sites are observed in the asymmetric unit, with the remainder of the $[Mo_8O_{26}]^{4-}$ anions being generated by a two-fold screw axis (see Figure 3). These anions, which stack in the [0 0 1] direction, are separated by protonated $[aqnH_2]^{2+}$ cations and occluded water molecules. A single $[aqnH_2]^{2+}$ cation is present in the asymmetric unit, while both [*R*-$aqnH_2]^{2+}$ and [*S*-$aqnH_2]^{2+}$ cations are generated through a series of inversion centers in the structure.

3. Four unique molybdenum sites are present in **3**, with the complete $[Mo_8O_{26}]^{4-}$ anion being generated by inversion

(19) Evans, O. R.; Lin, W. *Acc. Chem. Res.* **2002**, *35*, 511−522.
(20) Moulton, B.; Zaworotko, M. J. *Chem. Rev.* **2001**, *101*, 1629.
(21) Gutnick, J. R.; Muller, E. A.; Narducci Sarjeant, A.; Norquist, A. J. *Inorg. Chem.* **2004**, *43*, 6528.
(22) Muller, E. A.; Cannon, R. J.; Narducci Sarjeant, A.; Ok, K. M.; Halasyamani, P. S.; Norquist, A. J. *Cryst. Growth Des.* **2005**, *5*, 1913.
(23) *CrysAlis CCD* and *CrysAlis RED*, version 1.171; Oxford Diffraction Ltd.: Abingdon, U.K., 2002.
(24) Altomare, A.; Cascarano, G.; Giocovazzo, C.; Guagliardi, A. *J. Appl. Crystallogr.* **1993**, *26*, 343.
(25) Betteridge, P. W.; Carruthers, J. R.; Cooper, R. I.; Prout, C. K.; Watkin, D. J. *J. Appl. Crystallogr.* **2003**, *36*, 1487.
(26) Dowty, E. *ATOMS*, version 6.0; Shape Software: Kingsport, TN, 2002.
(27) Kurtz, S. K.; Perry, T. T. *J. Appl. Phys.* **1968**, *39*, 3798.
(28) Porter, Y.; Ok, K. M.; Bhuvanesh, N. S. P.; Halasyamani, P. S. *Chem. Mater.* **2001**, *13*, 1910.
(29) Kreusler, H. U.; Foerster, A.; Fuchs, J. *Z. Naturforsch. B* **1980**, *35*, 242.
(30) Lasocha, W.; Jansen, J.; Schenk, H. *J. Solid State Chem.* **1995**, *116*, 422.
(31) Lasocha, W.; Jansen, J.; Schenk, H. *J. Solid State Chem.* **1995**, *117*, 103.
(32) Lindqvist, I. *Ark. Kemi.* **1950**, *3*, 349.
(33) Harrison, W. T. A.; Stucky, G. D.; Gier, T. E. *Acta Crystallogr., Sect. C* **1993**, *49*, 1900.
(34) Muller, E. A.; Narducci Sarjeant, A.; Norquist, A. J. *Acta Crystallogr., Sect. E* **2005**, *61*, m730.

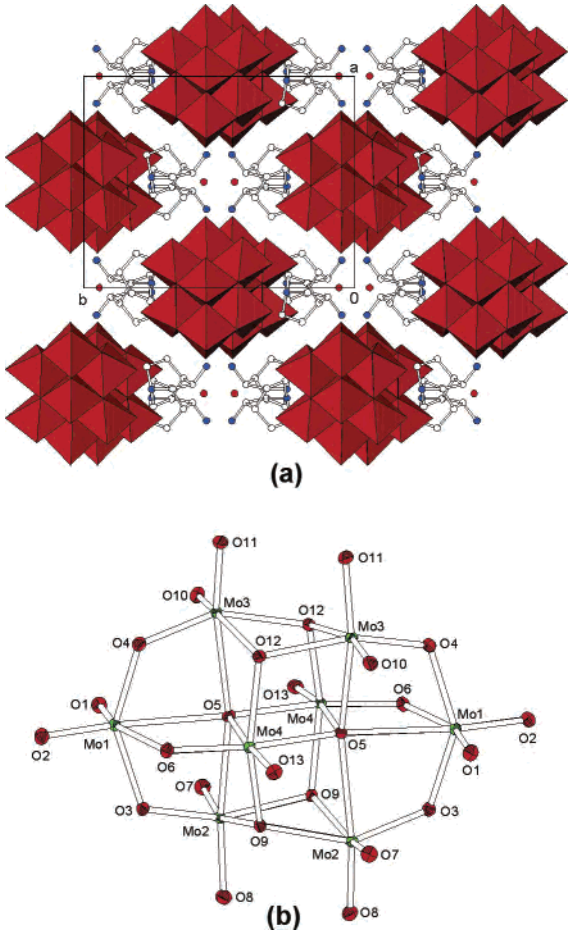

Figure 3. (a) Three-dimensional packing of **2**. Red octahedra represent MoO_6, while white, blue, and red circles represent carbon, nitrogen, and oxygen atoms, respectively. Hydrogen atoms have been removed for clarity. The unit cell is shown. (b) Thermal ellipsoid plot (50% probability) of the β-octamolybdate anion in **2**.

symmetry. Each $[Mo_8O_{26}]^{4-}$ anion shares two common oxide ligands with each of two neighboring $[Mo_8O_{26}]^{4-}$ anions, forming extended chains with a known connectivity.[35−37] These chains are aligned in the [1 0 0] direction and are separated by $[aqnH_2]^{2+}$ cations and occluded water molecules. Both $[R\text{-}aqnH_2]^{2+}$ and $[S\text{-}aqnH_2]^{2+}$ cations are generated through a series of inversion centers from a single $[aqnH_2]^{2+}$ cation in the asymmetric unit (see Figure 4).

4 and 5. Compounds **4** and **5** are closely related to one another. Each contains analogous β-octamolybdate anions, which are comprised of eight unique molybdenum sites and two distinct $[aqnH_2]^{2+}$ cations. The $[Mo_8O_{26}]^{4-}$ anions stack along the [1 0 0] direction and are separated by $[aqnH_2]^{2+}$ cations. **4** contains only $[R\text{-}aqnH_2]^{2+}$ cations, while **5** contains only $[S\text{-}aqnH_2]^{2+}$ cations. These two compounds both crystallize in the noncentrosymmetric space group $P2_1$ (No. 4), for which the only symmetry elements are a series of 2_1 screw axes (see Figure 5). The Flack parameters refined to −0.07(4) and −0.08(5) for **4** and **5**, respectively.

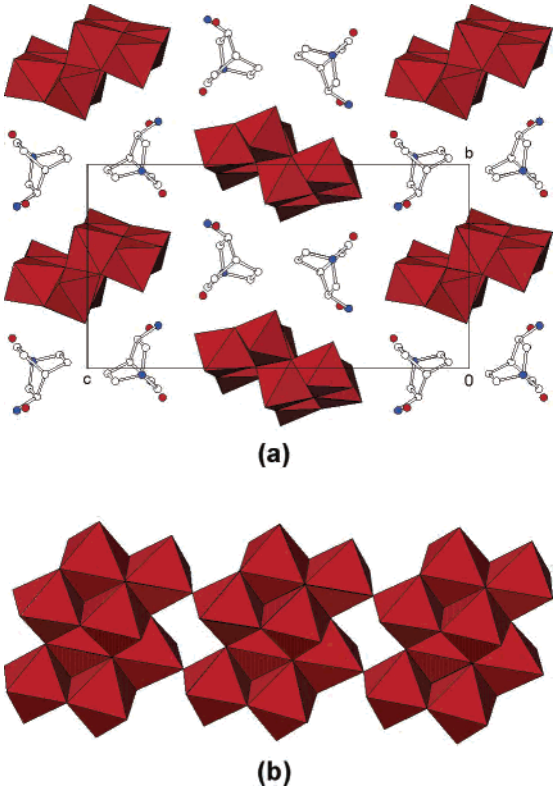

Figure 4. (a) Three-dimensional packing of **3**. Red octahedra represent MoO_6, while white, blue, and red circles represent carbon, nitrogen, and oxygen atoms, respectively. Hydrogen atoms have been removed for clarity. The unit cell is shown. (b) Polyhedral representation of the $[Mo_8O_{26}]_n^{4n-}$ chains in **3**.

Bond Valence Sums. The hydrogen-bonding networks present in **1**−**5** were analyzed using bond valence sums,[38] a method of quantifying both the relative strength and residual charge of each bond and respective ligand. All calculations were performed using parameters compiled by Brese and O'Keeffe.[39] The valence of each Mo−O and O−H bond was calculated (see Tables 2−6). The overall charge on each molybdenum center can be calculated by adding the appropriate bond valences. In each case, the molybdenum valences are close to 6+, the expected value. The relative residual negative charge on each oxide ligand can be calculated by adding the valences of each Mo−O and O−H bond in which a given ligand participates. The total bond valence ($\sum S_i$) is subtracted from the predicted valence of an oxide ligand, −2, to give the residual negative charge, which is related to the nucleophilicity of each ligand.[40−42] Oxide ligands that exhibit higher nucleophilicities have a greater propensity to accept a hydrogen bond from either the organic cations or occluded water molecules.[43] The residual negative charges on the oxide ligands vary considerably.

(35) Chakrabarti, S.; Natarajan, S. *Cryst. Growth Des.* **2002**, *2*, 333.
(36) Fang, R.-Q.; Zhang, X.-M.; Wu, H.-S.; Ng, S. W. *Acta Crystallogr., Sect. E* **2004**, *60*, m359.
(37) Thorn, K. J.; Narducci Sarjeant, A.; Norquist, A. J. *Acta Crystallogr., Sect. E* **2005**, *61*, m1665.
(38) Brown, I. D.; Altermatt, D. *Acta Crystallogr., Sect. B* **1985**, *41*, 244.
(39) Brese, N. E.; O'Keeffe, M. *Acta Crystallogr., Sect. B* **1991**, *47*, 192.
(40) Heier, K. R.; Norquist, A. J.; Wilson, C. G.; Stern, C. L.; Poeppelmeier, K. R. *Inorg. Chem.* **1998**, *37*, 76.
(41) Welk, M. E.; Norquist, A. J.; Stern, C. L.; Poeppelmeier, K. R. *Inorg. Chem.* **2000**, *39*, 3946.
(42) Welk, M. E.; Norquist, A. J.; Arnold, F. P.; Stern, C. L.; Poeppelmeier, K. R. *Inorg. Chem.* **2002**, *41*, 5119.
(43) Norquist, A. J.; Doran, M. B.; O'Hare, D. *Inorg. Chem.* **2005**, *44*, 3837.

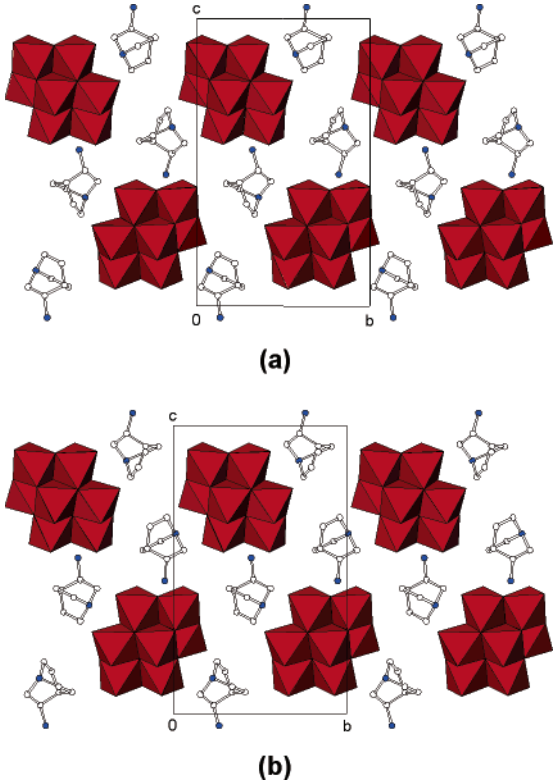

Figure 5. Three-dimensional packing in (a) **4** and (b) **5**. Red octahedra represent MoO_6, while white and blue circles represent carbon and nitrogen atoms, respectively. Hydrogen atoms have been removed for clarity. The unit cells are shown.

Table 2. Bond Valence Sums[a] for **1**

S_i	Mo1	Mo2	H atoms[b]	$\sum S_i$	$V - \sum S_i$
O1	1.58			1.58	−0.42[c]
O2	1.65			1.65	−0.35[c]
O3	0.91 × 2	0.37		1.77	−0.23[c]
		0.49			
O4	0.39	0.85 × 2		2.09	0.09
O5	0.44	0.84 × 2		2.12	0.12
O6		1.69		1.69	−0.31[c]
O7		1.74		1.74	−0.26
O8			0.8 × 5	1.6	−0.4[c]
$\sum S_i$	5.88	5.99			

[a] Valence sums calculated with the formula $S_i = \exp[(R_0 - R_i)/B]$, where S_i is the bond valence of bond i, R_0 is a constant dependent upon the bonded elements, R_i is the bond length of bond i, and B equals 0.37. $\sum S_i$ is the bond valence sum for each atom. V is the predicted valence for a site. $R_0(Mo^{VI}-O) = 1.907$. [b] O−H bond valences on occluded water molecules are approximated using $R_0 = 0.939$. [c] Hydrogen-bond acceptor (determined by N−O and O−O distances).

Calculation of the valences for O−H bonds in occluded water molecules is difficult because hydrogen atoms were placed in idealized positions with fixed bond lengths; therefore, accurate hydrogen atomic positions are not known. Approximations are included because the water molecules are important participants in the hydrogen-bonding structure, and neglecting the effects of the O−H valences on the oxide nucleophilicities leads to unreasonable values.

Composition Space Diagram. In a composition space diagram, the compositions of the crystalline products are plotted as a function of the reactant mole fractions. The total number of moles of MoO_3 and racemic aqn in each reaction was held constant, while the amount of solvent water was varied, creating a series of pseudobinaries. Any amorphous solids or soluble species after the reaction are neglected. Areas of selective crystallization, or "crystallization fields", are often observed. These diagrams are similar to binary phase diagrams in that the products are related to the initial reactant concentrations. However, solvent concentration replaces temperature in these diagrams. The final composition is not necessarily the same as the initial composition; therefore, composition space diagrams are not phase diagrams because they do not obey the phase rule.

Table 3. Bond Valence Sums for **2**

S_i	Mo1	Mo2	Mo3	Mo4	H atoms	$\sum S_i$	$V - \sum S_i$
O1	1.70					1.70	−0.30[a]
O2	1.68					1.68	−0.32[a]
O3	0.96	1.05				2.01	0.01
O4	1.01		1.03			2.04	0.04
O5	0.22	0.30	0.40	0.31		1.74	−0.26
				0.51			
O6	0.39			1.51		1.90	−0.10
O7		1.69				1.69	−0.31[a]
O8		1.76				1.76	−0.24[a]
O9		0.78		0.86		2.02	0.02
		0.38					
O10			1.75			1.75	−0.25
O11			1.69			1.69	−0.31[a]
O12			0.76	0.91		1.94	−0.06
			0.27				
O13				1.79		1.79	−0.21
O14					0.8 × 5	1.6	−0.4[a]
ΣS_i	5.96	5.96	5.90	5.89			

[a] Hydrogen-bond acceptor (determined by N−O and O−O distances).

Table 4. Bond Valence Sums for **3**

S_i	Mo1	Mo2	Mo3	Mo4	H atoms	$\sum S_i$	$V - \sum S_i$
O1	1.66					1.66	−0.34[a]
O2	1.76					1.76	−0.24
O3	0.91	0.83				1.74	−0.26[a]
O4	0.39	0.34	1.08			1.82	−0.18
O5	0.52		0.51	1.02		2.05	0.05
O6	0.74			1.36		2.10	0.10
O7		1.66				1.66	−0.34[a]
O8		1.70				1.70	−0.30[a]
O9		0.80		1.02		1.82	−0.18[a]
O10		0.44	0.25	0.37		1.95	−0.05
			0.89				
O11			1.79			1.79	−0.21[a]
O12			1.43	0.45		1.88	−0.12
O13				1.78		1.78	−0.22
O14					0.8 × 5	1.6	−0.4[a]
O15					0.8 × 5	1.6	−0.4[a]
$\sum S_i$	5.98	5.77	5.95	6.00			

[a] Hydrogen-bond acceptor (determined by N−O and O−O distances).

The composition space diagram for the MoO_3/aqn/H_2O system was constructed by conducting 36 distinct reactions. Reactant mole fractions were systematically varied; however, the total number of moles of MoO_3 and aqn was held constant at 5 mmol. An identical series of reactions was performed in four solvent water amounts: 0.5, 1.0, 1.5, and 2.0 g. In addition, a constant amount of 0.2 g of H_2SO_4 was added to each reaction to act as a mineralizer. The pH of each gel was adjusted to a value of 5 before the reaction, using concentrated NaOH and glacial acetic acid. Each reaction in this system was conducted using a racemic source of aqn.

The composition space diagram for the MoO_3/aqn/H_2O system, shown in Figure 6, has five distinct crystallization fields. In regions of high aqn concentrations, **1** is the only

Table 5. Bond Valence Sums for **4**

S_i	Mo1	Mo2	Mo3	Mo4	Mo5	Mo6	Mo7	Mo8	$\sum S_i$	$V - \sum S_i$
O1	1.76								1.76	−0.24
O2	1.71								1.71	−0.29
O3	0.93	1.02							1.95	−0.05
O4	0.86			1.04					1.90	−0.10[a]
O5	0.39		1.50						1.89	−0.11
O6	0.24	0.28	0.32	0.33		0.52			1.69	−0.31
O7		1.69							1.69	−0.31[a]
O8		1.74							1.74	−0.26[a]
O9		0.78			0.32	0.93			2.03	0.03
O10		0.36	0.83		0.77				1.96	−0.04
O11			1.80						1.80	−0.20
O12				1.68					1.68	−0.32[a]
O13				1.76					1.76	−0.24
O14			0.90	0.36			0.77		2.03	0.03
O15				0.73		0.73	0.37		1.83	−0.17[a]
O16					1.72				1.72	−0.28
O17					1.71				1.71	−0.29
O18			0.53		0.32	0.33	0.28	0.25	1.71	−0.29
O19					1.03			0.88	1.91	−0.09[a]
O20						1.77			1.77	−0.23
O21						1.55		0.37	1.92	−0.08
O22							1.76		1.76	−0.24
O23							1.73		1.73	−0.27[a]
O24							1.03	0.96	1.99	−0.01
O25								1.73	1.73	−0.27[a]
O26								1.79	1.79	−0.21
$\sum S_i$	5.89	5.87	5.88	5.90	5.87	5.83	5.94	5.98		

[a] Hydrogen-bond acceptor (determined by N−O distances).

Table 6. Bond Valence Sums for **5**

S_i	Mo1	Mo2	Mo3	Mo4	Mo5	Mo6	Mo7	Mo8	$\sum S_i$	$V - \sum S_i$
O1	1.81								1.81	−0.19
O2	1.73								1.73	−0.27[a]
O3	0.97	1.04							2.01	0.01
O4	0.87			1.02					1.89	−0.11[a]
O5	0.37		1.55						1.92	−0.08
O6	0.26	0.28	0.34	0.32		0.53			1.73	−0.27
O7		1.74							1.74	−0.26
O8		1.71							1.71	−0.29[a]
O9		0.78			0.37	0.90			2.05	0.05
O10		0.37	0.78		0.73				1.88	−0.12[a]
O11			1.76						1.76	−0.24
O12				1.70					1.70	−0.30
O13				1.75					1.75	−0.25
O14			0.93	0.33			0.77		2.03	0.03
O15				0.78		0.83	0.36		1.97	−0.03
O16					1.76				1.76	−0.24
O17					1.69				1.69	−0.31[a]
O18			0.53		0.33	0.32	0.28	0.24	1.70	−0.30
O19					1.03			0.86	1.89	−0.11[a]
O20						1.80			1.80	−0.20
O21						1.52		0.39	1.91	−0.09
O22							1.69		1.69	−0.31[a]
O23							1.72		1.72	−0.28[a]
O24							1.01	0.94	1.95	−0.05
O25								0.70	1.70	−0.30
O26								1.74	1.74	−0.26
ΣS_i	6.01	5.92	5.89	5.90	5.91	5.90	5.83	5.87		

[a] Hydrogen-bond acceptor (determined by N−O distances).

crystalline product. As the aqn mole fraction decreases and the MoO_3 mole fraction increases, a second region is observed in which both **1** and **2** cocrystallize. The third crystallization field, located at high MoO_3 and water concentrations, contains only **3**. As the MoO_3 concentration decreases, both **2** and **3** are observed in the reaction product. **2** is the dominant crystalline product over the remainder of the composition space.

SHG. The SHG intensities versus particle size for **4** and **5** are shown in Figure 7. Measurements were made on ground and sieved samples, with the 532-nm light quantified as a function of the particle size. **4** and **5** exhibit SHG efficiencies that are very similar to that of α-SiO_2, and neither compound is phase matchable.

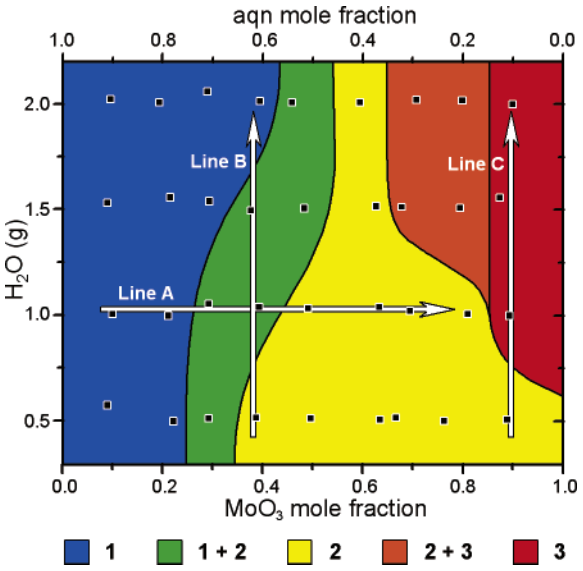

Figure 6. Composition space diagram for the MoO_3/aqn/H_2O system.

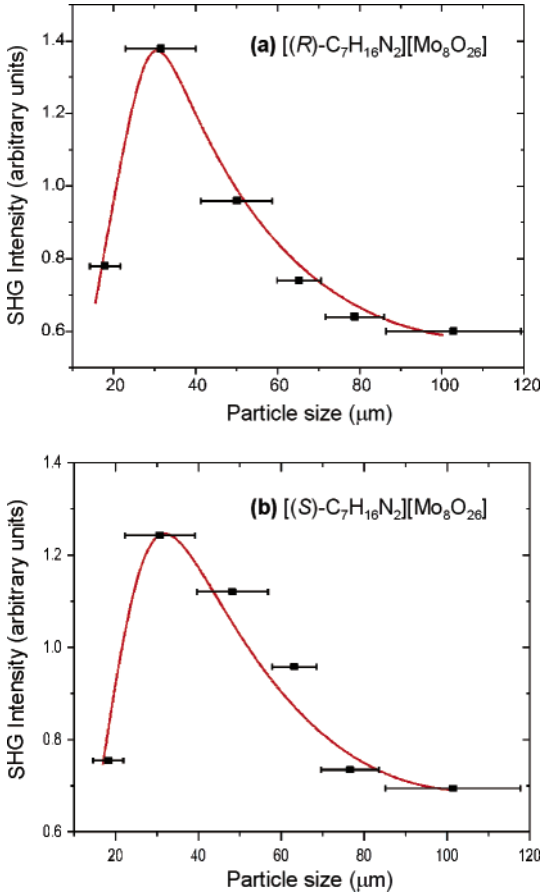

Figure 7. SHG intensity vs particle size for (a) **4** and (b) **5**. The curves drawn are to guide the eye and are not fits to the data.

Discussion

The construction of the composition space for the MoO_3/aqn/H_2O system serves two purposes. First, it provides a systematic means of investigating the types of compounds

that are formed from these reactants and the conditions under which they form. A wide variety of reaction conditions can be quickly scanned using an inexpensive racemic source of this chiral diamine. Second, the phase stability information gathered from the composition space can be used for targeted syntheses using enantiomerically pure aqn.

The composition space diagram for the MoO_3/aqn/H_2O system, shown in Figure 6, can be used to understand the phase stability of compounds **1**−**3**. In general, the compound whose composition most closely matches that of the reaction gel is the dominant crystalline product. This can be demonstrated through the investigation of molybdenum/template and molybdenum/H_2O ratios. The factors governing product composition can be elucidated through the investigation of three series of reaction, denoted Line A, Line B, and Line C in Figure 6.

Line A represents a series of reactions that were all conducted with 1 g of solvent water. **1** is the dominant crystalline product in the template-rich portion of Line A, with **2** and **3** being observed under molybdenum-rich conditions. This trend can be explained by comparing the compositions of **1**−**3**. **1** has a molybdenum/template ratio of 3:1, while both **2** and **3** have molybdenum/template ratios of 4:1. **1** dominates the crystallization in the template-rich portion of Line A because its composition more closely matches the reaction gel composition. In regions where the template concentration is high, the compound that incorporates more aqn is more likely to be stable. The template concentration decreases and the molybdenum concentration increases along Line A, which is reflected in the reaction product. A shift from phase-pure **1** to a mixture of **1** and **2**, phase-pure **2**, and a mixture of **2** and **3** is observed. The molybdenum-rich compounds, **2** and **3**, are present as products in the molybdenum-rich reactions, while the template-rich **1** is observed in aqn-rich reactions.

Line B represents a series of reactions in which the approximate aqn and Mo mole fractions are 0.6 and 0.4, respectively. The amount of solvent water varies from 0.5 to 2.0 g. In this series of reactions, the composition of the crystalline product is determined by the amount of solvent water because the molybdenum/aqn ratio present in these reactions is neither sufficiently molybdenum-rich to force crystallization of **2** or **3** nor so aqn-rich to force crystallization of **1**. Reactions with lower amounts of solvent water yield phase-pure **2**. As the amount of water increases, cocrystallization of **1** and **2** is first observed, followed by the production of phase-pure **1**. The molybdenum/H_2O ratio present in **1** and **2** can be used to understand this trend because the amount of molybdenum is fixed for each reaction on Line B. **1** exhibits a molybdenum/H_2O ratio of 3:1, while **2** has a molybdenum/H_2O ratio of 4:1. The compound that incorporates the greatest amount of solvent water in the structure for this fixed amount of molybdenum, **1**, dominates the crystallization in reactions with high water levels. Conversely, the compound with the lowest molybdenum/H_2O ratio, **2**, dominates the crystallization in reactions with low water levels. The intermediate region, in which **1** and **2** cocrystallize, is present in reactions of intermediate water levels.

Line C represents a series of reactions in which the molybdenum and aqn mole fractions are fixed at 0.9 and 0.1, respectively. The amount of solvent water varies between 0.5 and 2.0 g. The trend observed along Line C is analogous to what is present along Line B. **2** is formed in water-deficient conditions, while **3** forms in water-rich reactions. The molybdenum/H_2O ratio for **2** and **3** is 4:1 and 2:1, respectively. Again, the compound whose composition most closely matches that of the reaction gel tends to be the dominant crystalline product.

Composition space analysis not only can be used to understand the phase stability of the observed compounds but also can be used to control the composition of the inorganic component. $[Mo_8O_{26}]^{4-}$ anions and $[Mo_8O_{26}]_n^{4n-}$ chains exhibit a low amount of charge per molybdenum and are generally found in molybdenum-rich reactions. In contrast, $[Mo_3O_{10}]_n^{2n-}$ chains have a higher charge per molybdenum and are generally found in template-rich reactions. This trend should hold for related template systems and should allow for the efficient determination of the conditions necessary to cleanly synthesize the desired compounds. For example, compounds **4** and **5** were synthesized in good yield, without cocrystallization of other species, in a single reaction for each compound.

Several criteria were considered in the selection of the amine used for this study. First, the presence of a chiral center was necessary if any symmetry constraints are to be imposed on the reaction products. The availability of both racemic and enantiomerically pure samples of the same organic amine can enable one to control the inclusion of these symmetry constraints by conducting parallel experiments. Second, the use of a rigid diamine can deter orientational disorder within the organic amine, through the combination of low molecular flexibility and multiple points of interaction between the amine and inorganic components. Third, at least one of the amines within the molecule should be primary, to increase the degree of hydrogen bonding with the structure. 3-Aminoquinuclidine was selected because it fits each of these criteria. It is readily available as both a racemic mixture or just (*S*)-(−)-3-aminoquinuclidine or (*R*)-(+)-3-aminoquinuclidine and contains both a primary and tertiary amine, and its bicyclic nature provides rigidity within the molecule.

Elucidation of the role of $[aqnH_2]^{2+}$ cations in the crystallization of compounds **1**−**5** required a systematic investigation. Exploration of the composition space in the MoO_3/aqn/H_2O system resulted in the formation of three compounds synthesized from a racemic source of aqn and provided the necessary information to efficiently synthesize two additional compounds using enantiomorphically pure sources of either (*S*)-(−)-3-aminoquinuclidine or (*R*)-(+)-3-aminoquinuclidine. These five compounds form a basis from which the role of $[aqnH_2]^{2+}$ cations are discussed.

The role of the $[aqnH_2]^{2+}$ cations in compounds **1**−**5** is three-fold. First, the cations balance the charge on the anionic inorganic components. Second, the protonated amines create

an extensive hydrogen-bonding network. Third, the chirality of $[R\text{-aqnH}_2]^{2+}$ and $[S\text{-aqnH}_2]^{2+}$ affects the three-dimensional symmetry of the resulting compound if an enantiomerically pure source of the amine is used.

The inorganic components present in compounds **1**−**5** vary in connectivity and dimensionality. They do, however, all exhibit negative charge. The $[\text{aqnH}_2]^{2+}$ cations present in solution, while not the only source of positive charge in the reaction gel, are the lone source of charge balance that is incorporated into each compound.

The extensive hydrogen-bonding networks present in compounds **1**−**5** were investigated using bond valence sums (see Tables 2−6). The oxide ligands that accept hydrogen bonds in compounds **1**−**3** closely match those ligands with the greatest residual negative charge. This nucleophilicity is the primary factor governing the formation of the hydrogen-bonding network. Compounds **4** and **5**, however, contain apparent exceptions to this trend. At least one oxide ligand that exhibits a lower partial negative charge accepts a hydrogen bond in each of the latter two compounds when compared to the other oxide ligands. Geometric constraints are a secondary influence responsible for the donation of a hydrogen bond to a less nucleophilic oxide. Both compounds **4** and **5** contain two primary ammoniums, each of which donates three hydrogen bonds to neighboring oxides. For example, N2 in **4** donates hydrogen bonds to O4, O8, and O12. Two of these oxides, O8 and O12, are highly nucleophilic, while O4 has a lower residual negative charge. The formation of hydrogen bonds to O8 and O12, coupled with the steric influences dictating the H−N−H bond angles, limits the availability of hydrogen-bond acceptors. The position of O4, which is only moderately nucleophilic in the context of **4**, allows for the formation of three hydrogen bonds in the appropriate geometry. Similar geometries are observed for N4 in **4**, which donates hydrogen bonds to O19, O23, and O25. The environments around N2 and N4 in **5** are analogous to their counterparts in **4**. N2 donates hydrogen bonds to O17, O19, and O23, while N4 interacts with O2, O4, and O8.

Two trends, common to compounds **1**−**5**, were used to determine the structure-directing properties of the observed molybdate anions. First, the most nucleophilic oxides are generally those that either bind to a single molybdenum center or are shared by four or five molybdenums. The oxides that bridge between two or three molybdenum sites usually exhibit low nucleophilicities. Second, only the "accessible" oxides participate in hydrogen bonding. The four- and five-coordinate oxides do not accept hydrogen bonds because their positions within the anion generally preclude additional interaction for steric reasons. In contrast, the terminal oxides have no such constraints and freely accept hydrogen bonds. Therefore, $[\text{Mo}_8\text{O}_{26}]^{4-}$ anions and both $[\text{Mo}_8\text{O}_{26}]_n^{4n-}$ and $[\text{Mo}_3\text{O}_{10}]_n^{2n-}$ chains direct coordination through their terminal oxides, the most nucleophilic ligands that are accessible for interaction. While the complex hydrogen-bonding networks present in compounds **1**−**5** cannot be predicted, the interacting ligands can.

The structure-directing properties of the polyoxomolybdates discussed above are markedly different from those of related niobate anions. For example, it was demonstrated in a recent investigation that the bound hydrogen atoms on $[\text{Nb}_6\text{O}_{19}]^{8-}$ Lindquist ions in $\text{Na}_7[\text{HNb}_6\text{O}_{19}]\cdot 15\text{H}_2\text{O}$ are localized on bridging (two-coordinate) oxides.[44] Furthermore, oxygen exchange was shown to be most facile for bridging (two-coordinate) oxides, followed by terminal and central (six-coordinate) oxides. This behavior, while different from the polyoxomolybdate species presented here, can again be understood in the context of bond valence sums. The bridging (two-coordinate) oxides exhibit the largest residual negative charges, and so the hydrogen position is preferential to those sites. The oxygen valences and nucleophilicites also mirror the reported solvent exchange rates. A complete bond valence sum analysis of the $[\text{Nb}_6\text{O}_{19}]^{8-}$ anion[45] is listed in the Supporting Information.

Compounds **1**−**3** were synthesized from racemic sources of aqn, while **4** used (*R*)-aqn and **5** used (*S*)-aqn. The reaction gel compositions used to synthesize **4** and **5** were based upon an analysis of the MoO_3/aqn/H_2O composition space diagram, in which compound **2** is the dominant phase. Reaction conditions were selected to replicate those used in a phase-pure synthesis of **2**, allowing for a direct analysis of differences introduced through the use of either racemic or enantiomorphically pure sources of aqn.

Compounds **1**−**3** each crystallize in centrosymmetric space groups, while **4** and **5** both crystallize in the noncentrosymmetric space group $P2_1$ (No. 4). The use of enantiomerically pure sources of chiral organic amines in the syntheses of **4** and **5** precludes the formation of centers of inversion within these structures. A cancellation mechanism for the local distortions present in MoO_6 coordination octahedra cannot occur via the presence of extraframework centers of symmetry because the relationship of a $[R\text{-aqnH}_2]^{2+}$ cation through an inversion center requires a corresponding $[S\text{-aqnH}_2]^{2+}$ cation. The presence or absence of these enantiomers can be controlled; no $[S\text{-aqnH}_2]^{2+}$ cations can be incorporated into the resulting solid if $[R\text{-aqnH}_2]^{2+}$ cations alone are present in the reaction gel. $[R\text{-aqnH}_2]^{2+}$ cations can also never be related to one another through centers of inversion because the required $[S\text{-aqnH}_2]^{2+}$ cations are absent, prohibiting the formation of any such centers of symmetry. This constrains the space group of the solid to be noncentrosymmetric. The chirality of the $[R\text{-aqnH}_2]^{2+}$ and $[S\text{-aqnH}_2]^{2+}$ cations is reflected in the enantiomorphic and polar crystal class of these two compounds, **2** (C_2).

Compounds **2**, **4**, and **5** share two common structural components, β-octamolybdate anions and $[\text{aqnH}_2]^{2+}$ cations. However, the symmetry elements within these compounds differ considerably. The $[\text{Mo}_8\text{O}_{26}]^{4-}$ anions present in **2** reside on a series of two-fold axes of rotation at (0, y, $^1/_4$), with four unique molybdenum sites present. Neighboring anions are related to one another through inversion centers. The $[\text{Mo}_8\text{O}_{26}]^{4-}$ anions in **4** and **5** do not sit on any symmetry

(44) Alam, T. M.; Nyman, M.; Cherry, B. R.; Segall, J. M.; Lybarger, L. E. *J. Am. Chem. Soc.* **2004**, *126*, 5610.
(45) Goiffon, A.; Philippot, E.; Maurin, M. *Rev. Chim. Mineral.* **1980**, *17*, 466.

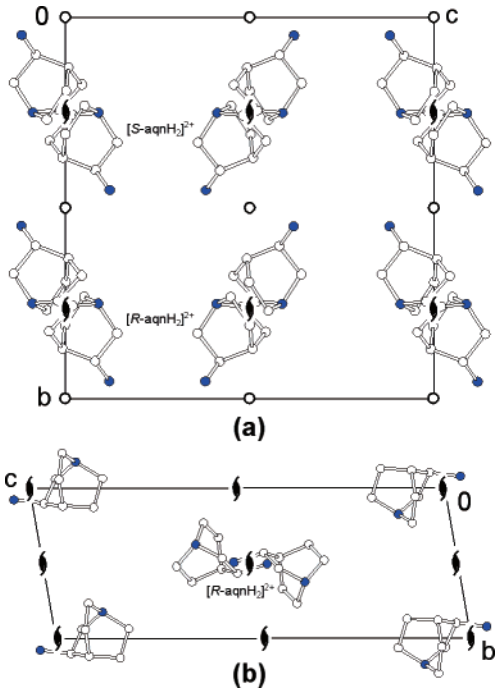

Figure 8. Cation structures in (a) **2** and (b) **4**. The symmetry elements present are shown. White and blue circles represent carbon and nitrogen atoms, respectively. Molybdenum, oxygen, and hydrogen atoms have been removed for clarity.

elements, and eight distinct molybdenum environments are present in each structure.

The asymmetric unit of **2** contains a single $[S\text{-aqnH}_2]^{2+}$ cation, from which $[R\text{-aqnH}_2]^{2+}$ cations are generated by inversion centers. **4** and **5** both contain two complete $[\text{aqnH}_2]^{2+}$ cations, either two $[R\text{-aqnH}_2]^{2+}$ or two $[S\text{-aqnH}_2]^{2+}$ cations, respectively. These $[\text{aqnH}_2]^{2+}$ cations are aligned along 2_1 screw axes in each of these three compounds (see Figure 8). In each compound, any given column of cations contains either $[R\text{-aqnH}_2]^{2+}$ or $[S\text{-aqnH}_2]^{2+}$ cations. Mixtures of both enantiomers along a given 2_1 screw axis are not observed. However, the formation of a series of inversion centers in **2** is allowed, relating neighboring stacks of $[R\text{-aqnH}_2]^{2+}$ to $[S\text{-aqnH}_2]^{2+}$. No such centers of symmetry can be present in **4** or **5**, and different cation chemical environments are observed between **2** and compounds **4** and **5**.

The forced absence of inversion centers from **4** and **5**, a result of the presence of only a single $[\text{aqnH}_2]^{2+}$ enantiomer, imparts a reduction of symmetry upon the $[Mo_8O_{26}]^{4-}$ anions and forces the β-octamolybdate anions to pack in a noncentrosymmetric arrangement. The possibility of pseudosymmetry with the inorganic components of **4** and **5** was investigated. The $[\text{aqnH}_2]^{2+}$ cations were removed from the crystallographic models, and Platon[46] was used to probe for missing symmetry. None was found, confirming the ability of chiral cations to impart noncentrosymmetry in inorganic structures. Possible mechanisms for the formation of inversion centers within such structures do exist. Crystallographic disorder of the chiral cation or the formation of an incommensurate crystal can result in centrosymmetry.

The viability of using chiral organic amines to constrain the reaction product symmetry is demonstrated in the nonlinear-optical activity of **4** and **5**. The measured SHG response in these two compounds validates this strategy for the formation of new noncentrosymmetric materials.

Conclusion

Understanding the factors governing product composition, hydrogen bonding, and symmetry can lead to control of the hydrothermal reaction products and the rational design of new functional materials. We demonstrated control over both symmetry and composition in the targeted syntheses of the SHG-active **4** and **5**, through the use of composition space analysis and either racemic or enantiomerically pure 3-aminoquinuclidine. Bond valence sums were used to determine the structure-directing properties of the observed molybdates, which are integrally important in the formation of the observed hydrogen-bonding networks.

Acknowledgment. This research was supported by an award from Research Corp. and the David and Lucile Packard Foundation. A.N.S. gratefully acknowledges support from the National Science Foundation (Award No. CHE-0215963). K.M.O. and P.S.H. thank the Robert A. Welch Foundation, the NSF-Career Program (Grant DMR-0092054), and the NSF-Chemical Bonding Center for support.

Supporting Information Available: X-ray crystallographic file containing complete tables of atomic coordinates, thermal parameters, and bond lengths and angles for **1**−**5** (CIF), figures of thermal ellipsoid plots, a table of bond valence sum details, and a figure of the $[Nb_6O_{19}]^{8-}$ anion (PDF). This material is available free of charge via the Internet at http://pubs.acs.org.

IC060558T

(46) Spek, A. L. *J. Appl. Crystallogr.* **2003**, *36*, 7.